The Latest (Dusty) Pieces in the Rosetta Story

Stavro L. Ivanovski
INAF – Astronomical Observatory of Trieste
stavro.ivanovski@inaf.it

on behalf of the Rosetta Dust Group

Rosetta Dust Group:
Discriminating Properties (fingerprints of 67P dust particles) and considered instruments

Isotopic Ratios | **Structure and Porosity**
Grain Size Distribution | **Composition**
Albedo (opt. properties) | **Thermal Properties**

GIADA | **MIDAS** | **COSIMA**
Modelling | **OSIRIS** | **VIRTIS**
Stardust | **ROSINA**

Topics:

Dust Phase Function
Dust classification
Dust Charging
3D+t dust modelling
How comet works
Ground-based observations

Isotopic Ratios

COSIMA

- $^{34}S/^{32}S$: 0.0463 ± 0.006
- $\delta^{34}S$ = (+41 ± 130)‰ Paquette et *al*. (2017)

- $^{18}O/^{16}O$: 2.00 x 10^{-3} ± 1.2 x 10^{-4}
- $\delta^{18}O$ = (–2.6 ± 60)‰ Paquette et *al*. (2018)

- D/H: (1.41 ± 0.12) x 10^{-3}
- δD = (+8050 ± 800)‰ To be submitted soon

- $^{13}C/^{12}C$: 0.0134 ± 6.1 x 10^{-4}
- $\delta^{13}C$ = (+136 ± 55)‰ Preliminary; TBC

ROSINA

- $^{29}Si/^{28}Si$ = 0.0385 ± 0.0148
- $\delta^{29}Si$ = (-242 ± 291)‰ Rubin et *al*., (2018)

- $^{30}Si/^{29}Si$ = 0.588 ± 0.208
- $\delta^{30}Si/^{29}Si$ =(-108 ± 315)‰ Rubin et *al*., (2018)

- Other sputtered materials seen are Na, Ca, and K.

No isotopic ratios quoted for Ca or K. Interferences masked ^{24}Mg, ^{27}Al, ^{48}Ti

Message: we need also **Stardust**

Due to Sharing Geoscience Online format of EGU 2020 only selected recently published results (2019/2020) are displayed in this presentation

6 May 2020, S. Ivanovski, EGU2020

Isotopic Ratios

COSIMA

Measuring the $^{13}C/^{12}C$ Ratio with COSIMA (Paquette, J et al. EPSC-DPS2019-1338-2, 2019)

For the olivine: $^{13}C/^{12}C = 0.0125 \pm 2.5 \times 10^{-3}$

For the spectra of cometary dust with C > CH_3: $^{13}C/^{12}C = 0.0134 \pm 6.1 \times 10^{-4}$

Quoted errors are 1-sigma (but seem a bit small to me)

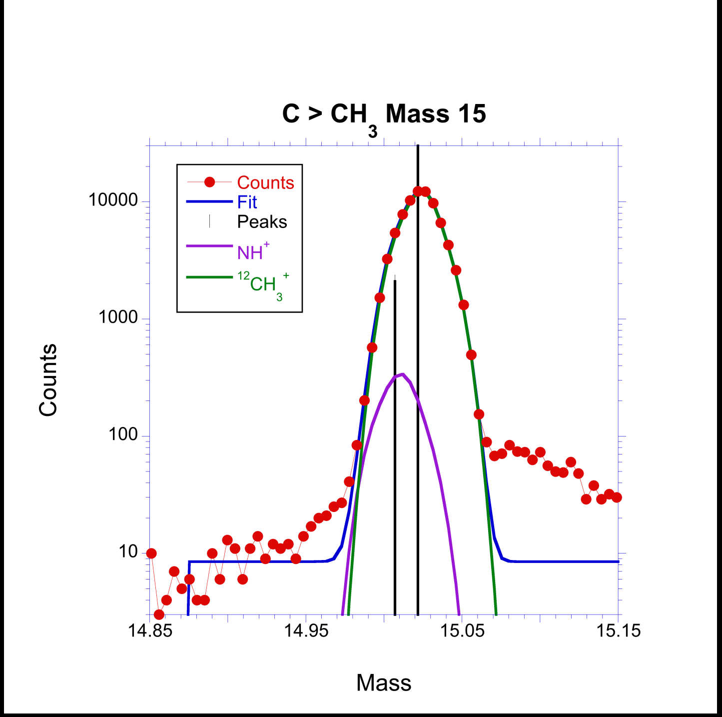

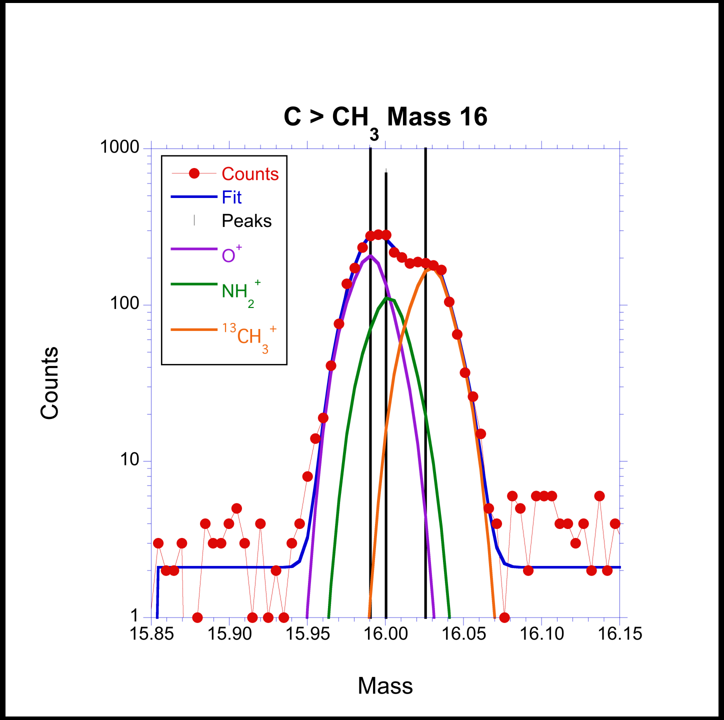

Step 1. Fit masses 15 and 16

Step 2. Subtract off normalized target contribution

$X_{net} = X_{sample} - (PDMS_{sample}/PDMS_{target}) \times X_{target}$

Doing so about 57% of the $^{12}CH_3$ counts and about 50% of the $^{13}CH_3$ counts are from the sample

Figs. In this case 79% of $^{12}CH_3$ counts and 75% of $^{13}CH_3$ counts are from the cometary dust

Grain Size (Distribution)

MIDAS VIRTIS OSIRIS

- MIDAS: Smallest features in high resolution images 90-100nm in size (Mannel et al. 2019, A&A).
- VIRTIS: Observe superheating in outbursts, can be explained by ejection of small grains. Size assumed to be ~100nm (Bockelée-Morvan et al.2017, MNRAS)
- OSIRIS phase function: “Smile” shape might indicate scattering at small features on the surface of large grains.
- All indications are towards ‘a single size’, not a distribution
- Stardust
- Open questions: Are these smallest observed particles the real fundamental building blocks? Or do we still look at small agglomerates?

Message: smallest sizes by MIDAS fit CP IDP subunit sizes

Due to Sharing Geoscience Online format of EGU 2020 only selected recently published results (2019/2020) are displayed in this presentation

6 May 2020, S. Ivanovski, EGU2020

Grain Size (Distribution)

MIDAS

DUST COLLECTED AT 67P BY MIDAS: FEATURES AT THE NANOMETRE SCALE

Mannel et al. 2019, A&A

Smallest features in dust of comet 67P determined by MIDAS in particle G:

- Differential sizes follow (log-)normal distributions
- Mean value between 90 and 100nm, standard deviation between 20 and 35 nm
- Small features seem to comprise next larger features with sizes about 400nm
- Smallest sizes in agreement with CP IDP subunit sizes, but on the smaller side and narrower distributed
- Fine Stardust material shows slightly different size distributions

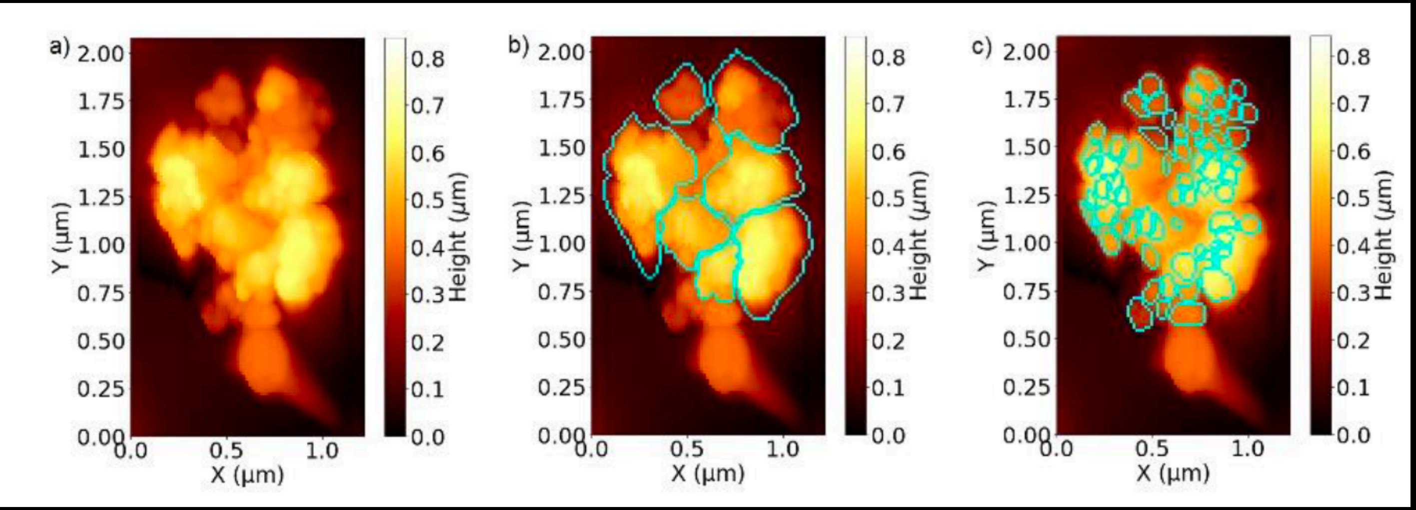

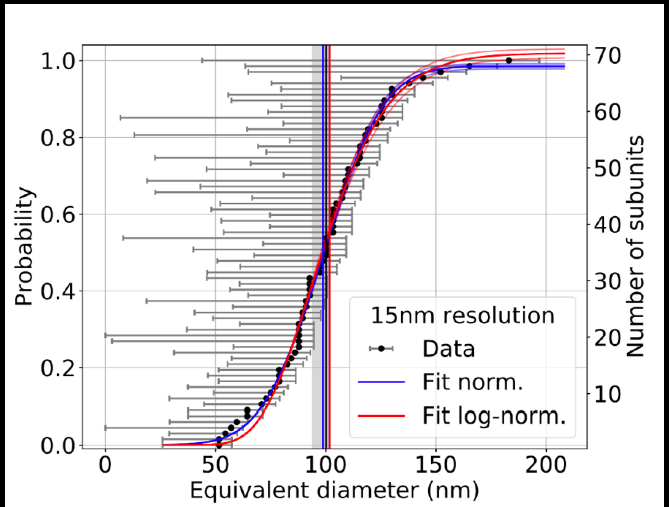

Differential size distributions of the subunits of CP IDPs also follow log-normal distributions:

- 5600 subunits of 4 CP IDPs: geometric means between 68 and 306 nm (sd between 16 and 137 nm) (Wozniakiewicz et al. 2013)
- 100 subunits of 1 CP IDP: Mean of 585 with 100nm sized units most frequently detected (Rietmeijer 1993).
- Means and distributions in agreement, although MIDAS subunits on the small side. Width of MIDAS subunit distribution noticeably small.

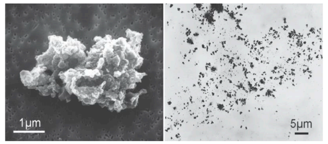

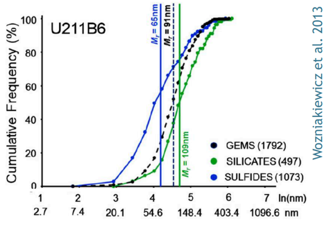

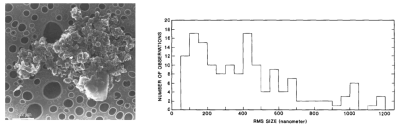

Rietmeijer et al. 1993

Differential size distribution of MIDAS 100nm sized surface features follow a (log-)normal distribution.

6 May 2020, S. Ivanovski, EGU2020

Structure and Porosity

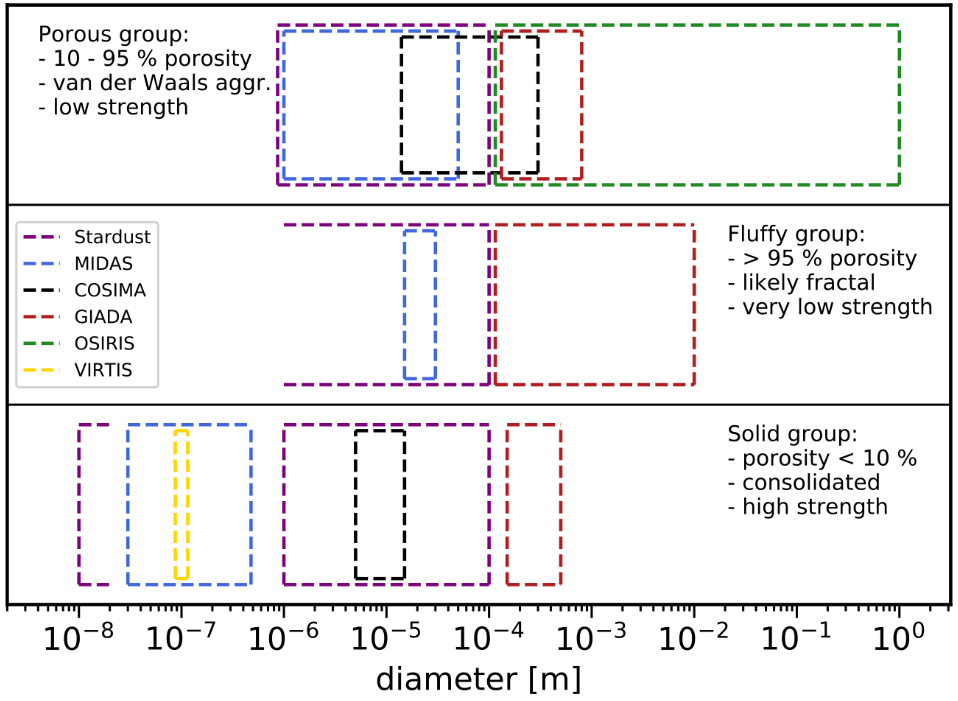

Fig. 12. Visual representation of Table 1 to show where different instruments have overlaps in their sensitivity range. Open boxes denote unknown size limits, i.e., smaller equal or larger equal than the plotted size.

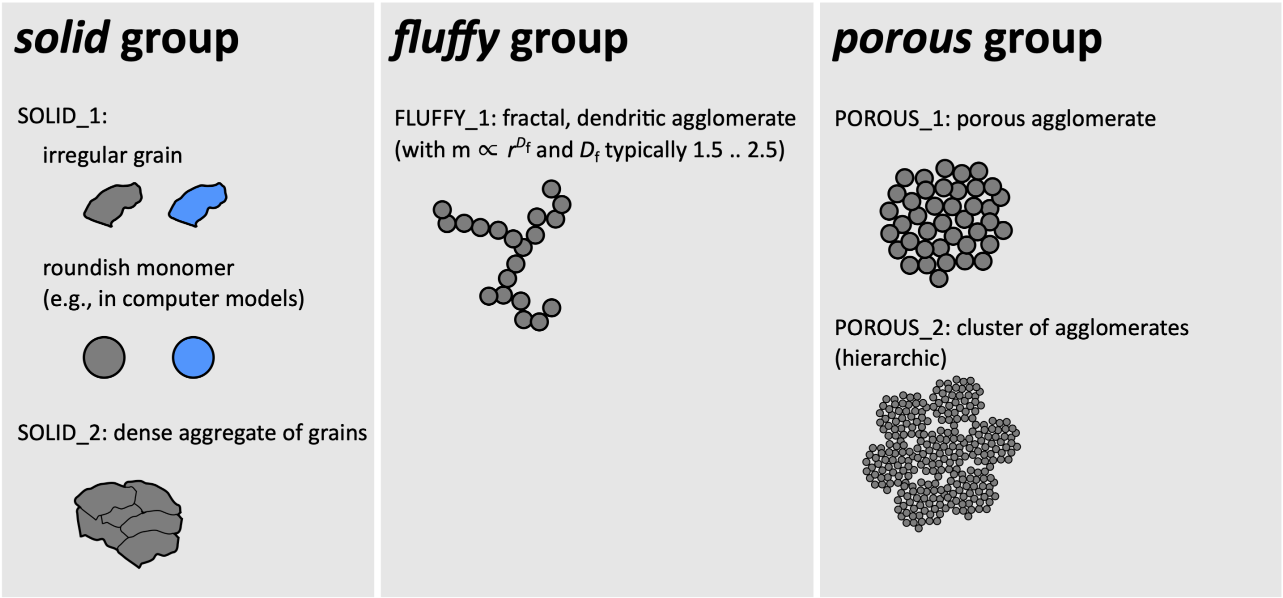

Fig. 1. Possible dust-particle structures, applying the three main groups defined in Sect. 2.2. The units of larger structures are drawn from circles for illustrative purposes only. In reality, these can be any of the *solid* group, where also colours (grey and blue) indicate that compositions can vary (e.g., ices).

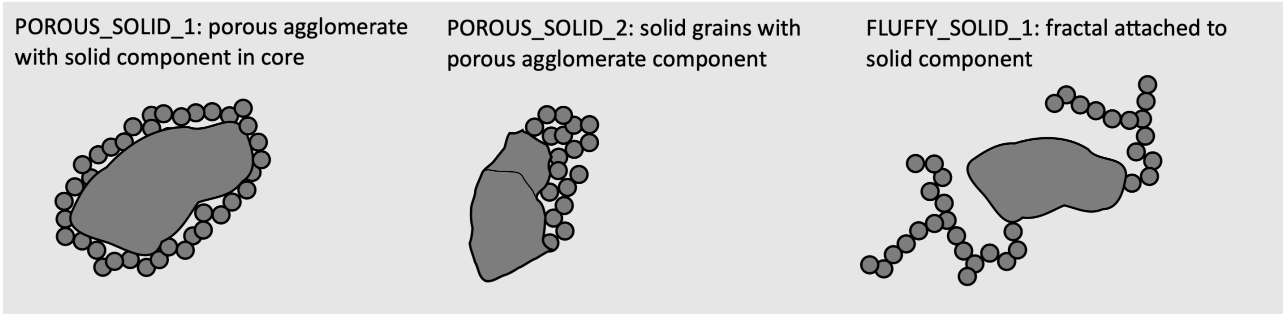

Fig. 7. The classification from Sect. 2.2 and Fig. 1 is not always unambiguous. These examples of **mixed cases** show aggregate structures that would be classified one way or another depending on the method applied (e.g., surface microscopy vs. mass determination vs. light scattering)

Rosetta and Stardust classification of dust particles (Guettler et al., 2019,A&A)

6 May 2020, S. Ivanovski, EGU2020

Structure and Porosity

	MIDAS	COSIMA	GIADA	OSIRIS	VIRTIS	Stardust
***porous* group** - porosity 10-95 % - aggregate - low strength	1 – 50 μm	14 – 300 μm on target; up to mm-range parents	0.1 – 0.8 mm	~100 μm – 1 m dominant scatterers	dominating size distribution (diff. slope –2.5 to –3)	particle creating track A with multiple terminals or track B 1 – 100 μm
***fluffy* group** - porosity >95 % - likely fractal - very low strength	fractal: 15 – 30 μm $D_f = 1.7 \pm 0.1$ constituent particles: < 1.5 μm	no indication	0.1 – 10 mm $D_f < 1.9$, ~23 % of GDS detections	not dominant scatterers	not excluded, consistent with moderate super-heating in normal activity	particle creating bulbous tracks (B for coupled, A* or C for fluffy GIADA detections), aluminium foil clusters. Up to 100 μm
***solid* group** - porosity <10 % - consolidated - high strength	50 – 500 nm fragments collected on tip	CAI candidate and specular reflection 5 – 15 μm	0.15 – 0.5 mm ~4000 kg m^{-3}	no indication	outburst: temperature requires 0.1 μm particles	particle creating track A with single or multiple terminals, 10s of nm, 1 – 100 μm

Message: Rosetta and Stardust classification of dust particles (Guettler et al., 2019, A&A)

Structure and Porosity

- Scattering of dust particles: phase function and polarization
  - Optical properties of the dust particles (**Langevin et al., 2020,PSS**)
    -> a median value of 9% for the reflectance factor of COSIMA particles, closer to that from OSIRIS (5–7%) than the initial evaluation (10.8%)
  - Fit of the phase function with dirty cotton ball (**Munoz et al. 2020, A&A**)
    -> porous and non spherical
  - Reproducing the linear polarization (**Levasseur-Regourd et al. 2019, A&A**)
    -> irregular particles with porosity 60% to 70%

- In situ measurements
  - Charging of dust particles under In+ beam (**Hornung, K et al. 2020,PSS**)
    -> permitivity -> porosity 0.7 to 0.9
  - Fluffy and compact particles on 67P nucleus (**Longobardo et al., 2019, MNRAS**)
    -> compact and fluffy particles are emitted contemporarily from common nucleus surface areas, later spread during the motion due to their different velocities.

Message: Particles cover all porosities -> structure

Due to Sharing Geoscience Online format of EGU 2020 only selected recently published results (2019/2020) are displayed in this presentation

6 May 2020, S. Ivanovski, EGU2020

Structure and Porosity

Dust Phase Function

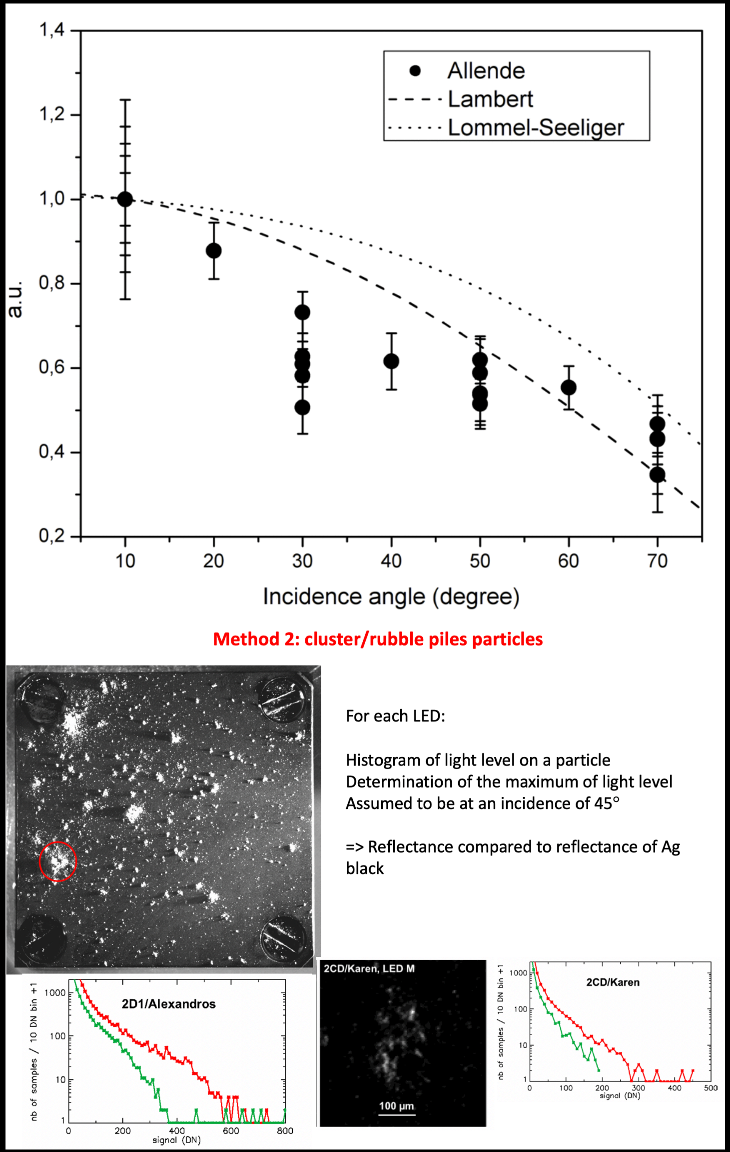

Optical properties of the dust particles (Langevin et al., 2020,PSS)

- Laboratory measurements of reflectance properties of **analog materials** to check the **validity of the scattering model** used to interpret COSIMA data
- Measurements on **SiO_2 aggregates** and **Tagish Lake fragments** -> the model was validated on SiO_2 aggregates; Tagish showed too large heterogeneities to be measured; the model was also validated on Allende powder.

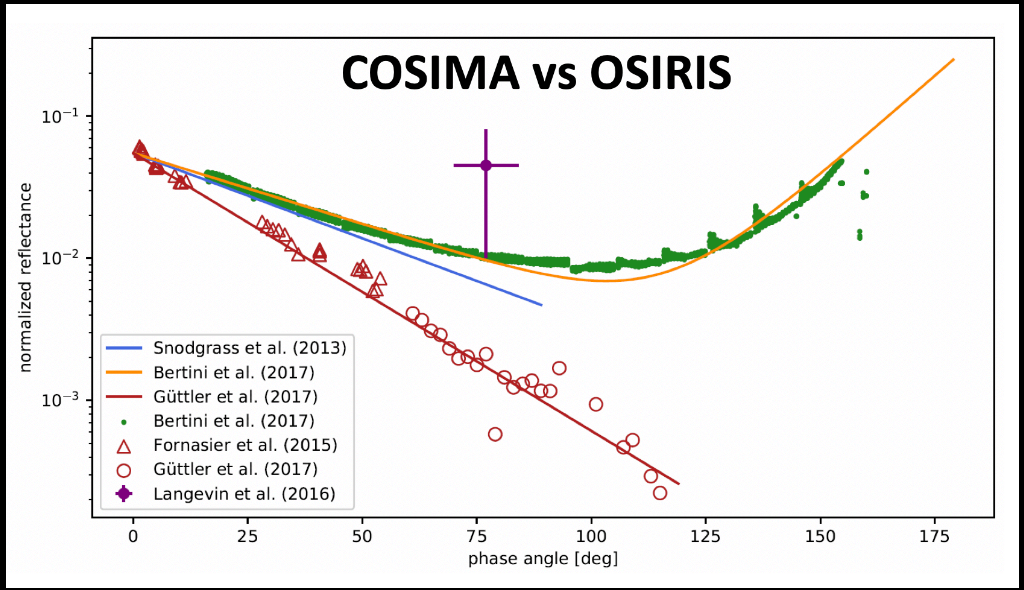

Shadowing on the nucleus that would have made it darker? (Vincent et al. 2019)

That could account for up to 22% of the darkening

Decrease of the reflectance derived by COSIMA by a factor of about 1.5

Structure and Porosity | Dust Phase Function | Ground-based obs.

What type of dust grains can reproduce the OSIRIS phase functions and ground-based observations of the degree of polarization? (Munoz et al. 2020, A&A)

IAA COSMIC DUST LABORATORY
PF & DLP by mm-sized grains setup

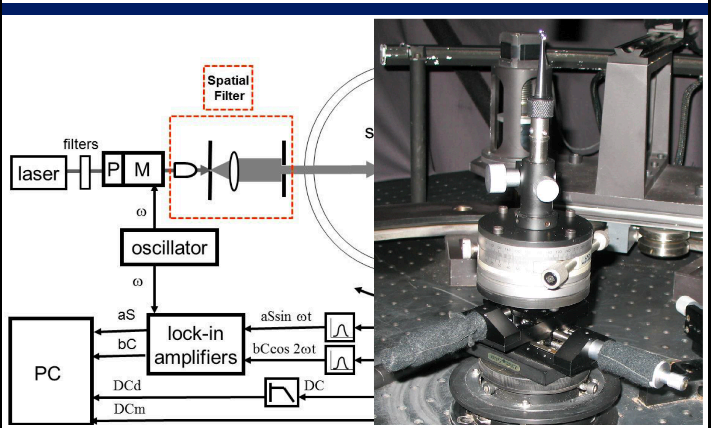

Experiments: Dust grains in random orientation

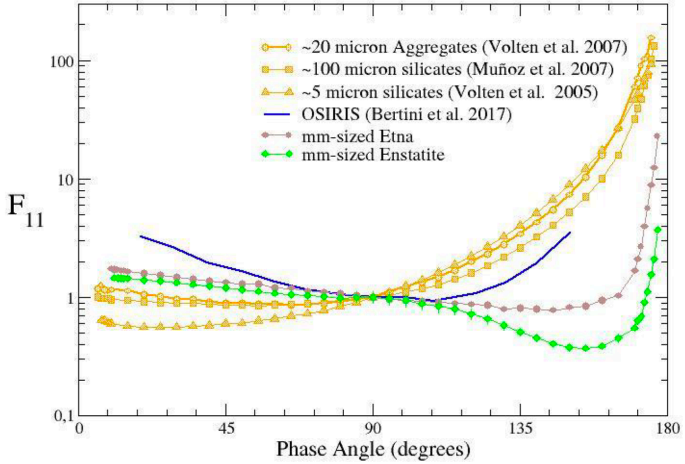

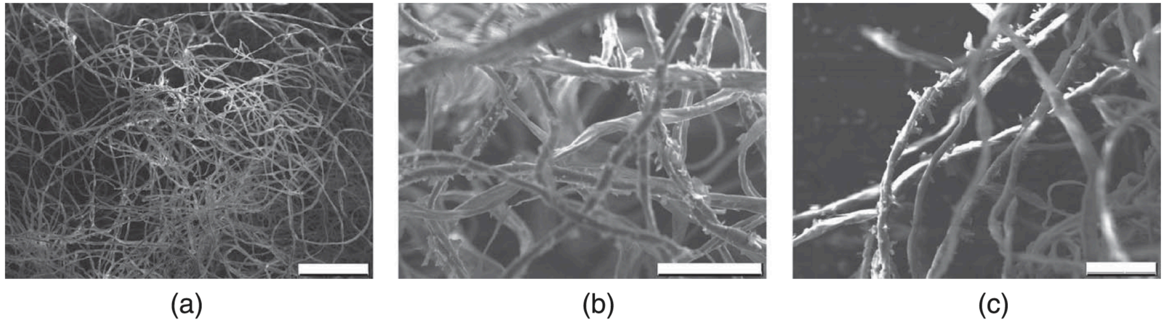

Figure 9. SEM images of the dirty cotton ball grain. White bars denote (a) 500 μm and (b, c) 100 μm. Small particles covering the cotton fibers correspond to the charcoal inclusions.

THE ASTROPHYSICAL JOURNAL SUPPLEMENT SERIES, 247:19 (13pp), 2020 March — Muñoz et al.

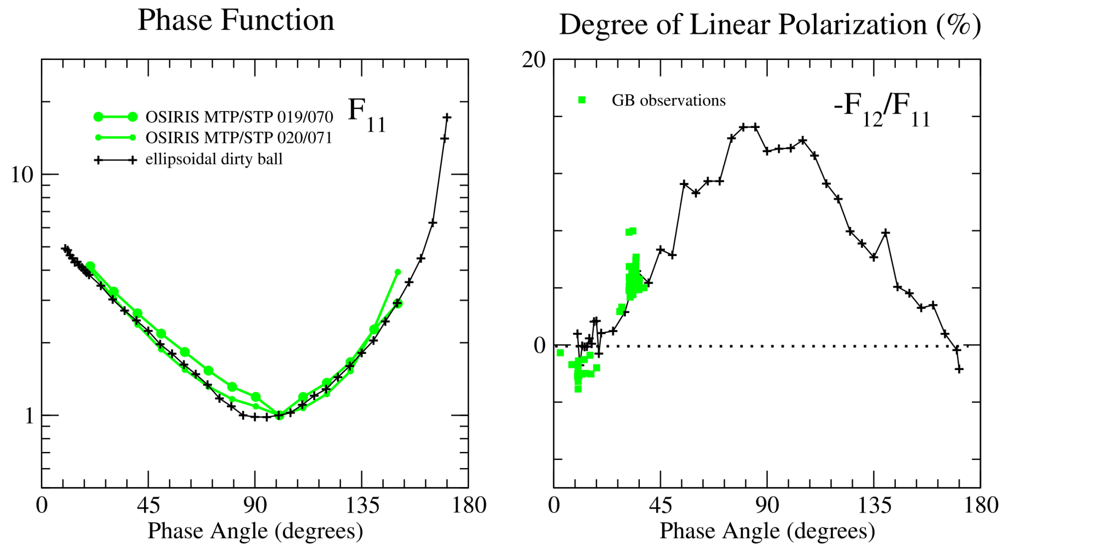

Figure 17. Green symbols correspond to the OSIRIS phase functions from Bertini et al. (2017) (left panel) and observed DLP for 67P from Rosenbush et al. (2017) and references therein (right panel). The observations are presented together with the measured phase functions and DLP for the flattened dirty cotton ball at a fixed orientation (δ_0). All F_{11} curves are normalized to unity at $\theta = 100°$.

Conclusion: mm-sized absorbing porous particles in fixed orientation

Due to Sharing Geoscience Online format of EGU 2020 only selected recently published results (2019/2020) are displayed in this presentation

Structure and Porosity

Dust Phase Function

Interpretation of phase curves within 67P inner coma through PROGRA2 experimental simulations (Levasseur-Regourd et al., 2019, A&A)

PROGRA2-Vis

Brightness & linear polarization of levitating dust particles

- Halogen white lamps, depolarizing filter, spectral filters (553±30 nm, 650±30 nm)
- Dust particles within a rotating vial
- Beam-splitter cube
- 2 synchronized cameras and one reference camera
- For particles > 20 µm and mixtures, measurements under µ-gravity conditions

E.g., *Renard et al. 2002; ACLR et al. 2015.*

Proportion of fluffy aggregates vs more compact ones constant in mass (35 ± 10 % vs 65 ± 10%)
Not too different from ≈ 37% in volume for very porous fractal particles *(Fulle and Blum 2017)*
or from ≈ 35% in counts of type C dust tracks by Stardust *(Burchell et al. 2008)*

Black carbon fluffy aggregates
Sizes ≈ 100 µm
Monomers of 14, 25, 56 and 90 nm

Porous volcanic ashes
Eyjafjallajökull & Lokon (sizes < 50 µm),
Also from Etna (sizes ≈ 50, 100 and 200 µm)

Crushed meteoritic dust
Sizes < 200 µm
One achondrite (aubrite)
Three carbonaceous chondrites
(Orgueil, Allende, North Africa)

Interplanetary dust analogues
Carbonaceous & mineral compounds
(ratios changing from one another)

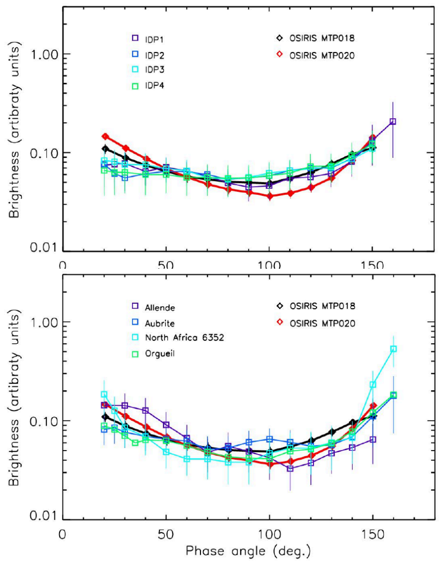

Results
2. Flattened U-shaped curves
Tentative analogues

Quite satisfactory fits for previous analogues for the interplanetary dust in the ecliptic, with clues to sublimation from 1.5 0.3 au
(Hadamick et al, PSS in press)

First laboratory measurements showing flattened U-shaped curves?

Quite satisfactory fits for crushed meteorites, and specially for carbonaceous ones as Orgueil
(from aggregates with sizes ≈ 10s µm)

Past numerical developments in polarimetry with 1P/Halley and C/1995 O1 Hale-Bopp
Satisfactory polarimetric fits for fluffy aggregates of irregular submicron-sized grains grains, mixed with compact particles, and composed of minerals and absorbing carbonaceous material *(Lasue et al. 2009)*.

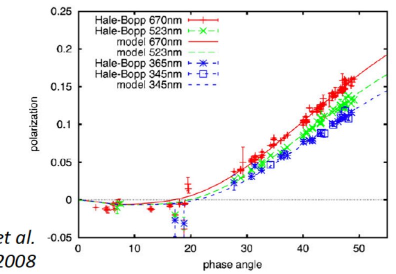

ACLR et al. PSS 2008

Numerical simulations for 67P, as compared to Ivano Bertini brightness phase curves

- Satisfactory fits for absorbing particles, with sizes ≈ 20 µm, porosity in the 60-70% range, and further assumptions on their orientation *(Moreno et al., 2018)*.
- Excellent agreement for irregular particles, with sizes in the 5-20 µm range, composed by an intimate mixture of sub-µm organic material and µm-sized spherical silicate grains *(Markkanen et al., 2018)*.

→ Results converging towards particles with sizes of about tens of micrometers, consisting of organics-rich mixtures.

Due to Sharing Geoscience Online format of EGU 2020 only selected recently published results (2019/2020) are displayed in this presentation

6 May 2020, S. Ivanovski, EGU2020

Structure and Porosity | **Dust Charging**

Charging of dust particles in-situ with COSIMA (Hilchenbach, M. et al TBS; Hornung, K. et al 2020,PSS)

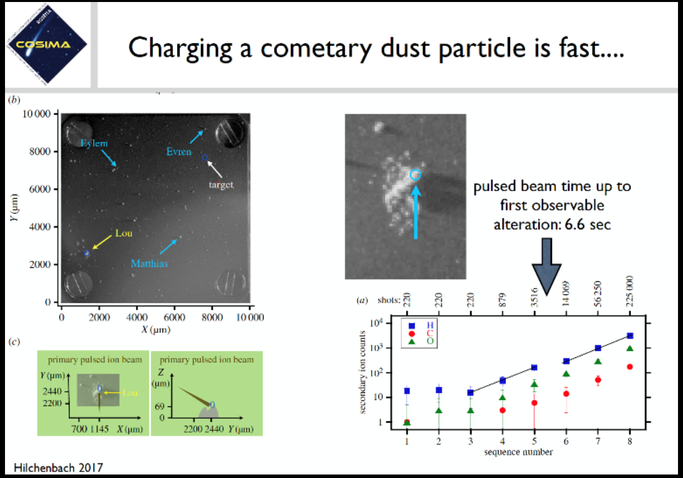

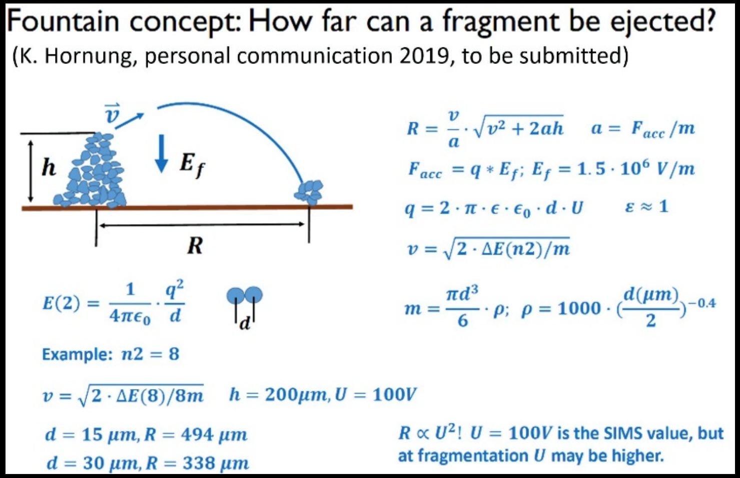

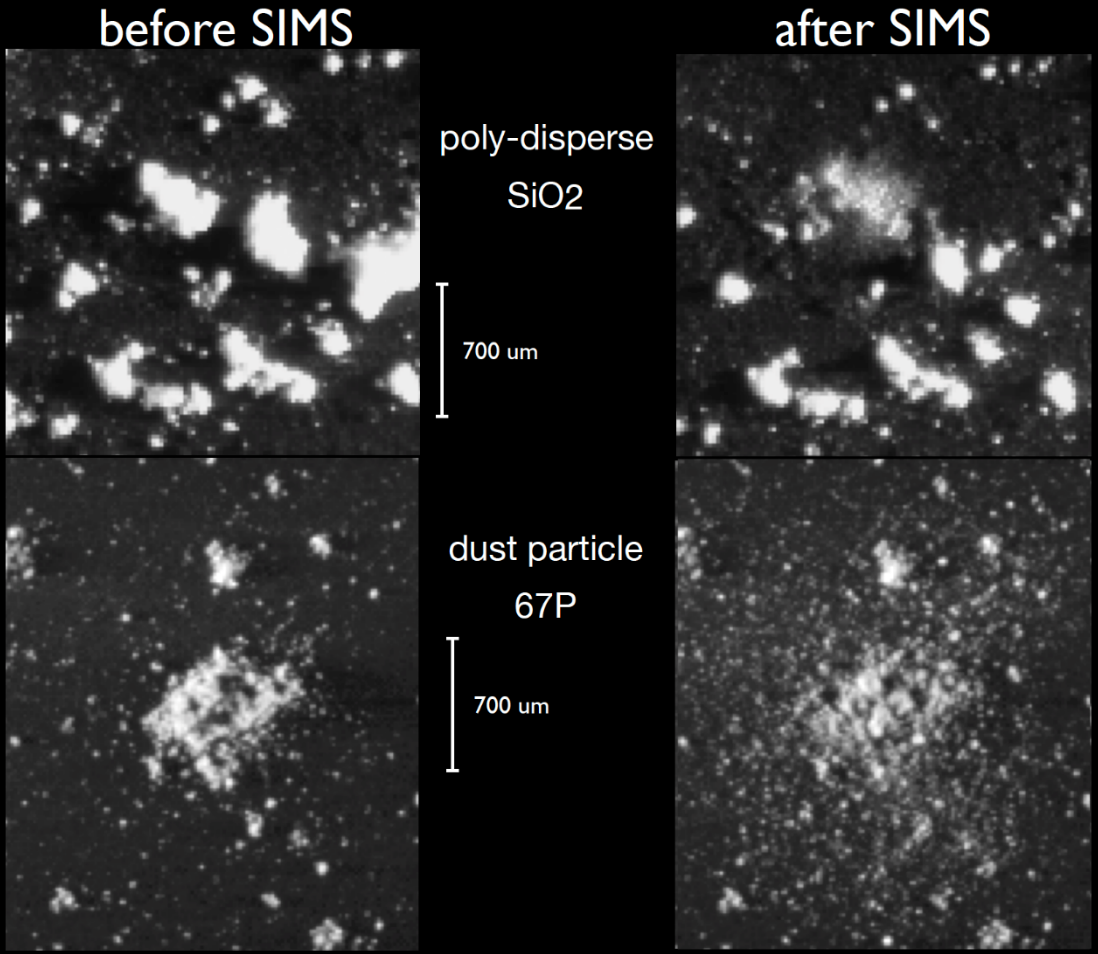

The composition data of the dust collected by COSIMA show that it has a mineral-to-organic ratio of ≈ 0.55/0.45 by weight (Bardyn et al. 2017) or ≈ 0.3/0.7 by volume assuming a density ratio mineral/organic of ≈ 3 (Greenberg and Li 1999).

The organic part of the investigated particles is found to have high molecular weight (Fray et al. 2016) and typical permittivities for such materials are $\varepsilon_r \approx 2$ (Chanda 2018).

Mineral values show a greater variety ranging from ≈ 4 (Silica) up to ≈8 (Olivine) and ≈ 8.5 (Pyroxene), (e.g. Zheng et al. 2005).

- cometary dust is a very bad conductor (specific resistivity $> 1.2 \cdot 10^{10}\,\Omega m$).
- the relative permittivity upper limit: $\varepsilon_r < 1.2$ sets a lower boundary for the porosity: $P > 0.8$ of particles $< 50\mu m$.

Due to Sharing Geoscience Online format of EGU 2020 only selected recently published results (2019/2020) are displayed in this presentation

6 May 2020, S. Ivanovski, EGU2020

Structure and Porosity

67P dust activity before perihelion identified by GIADA and VIRTIS data fusion (Longobardo et al. 2019, MNRAS)

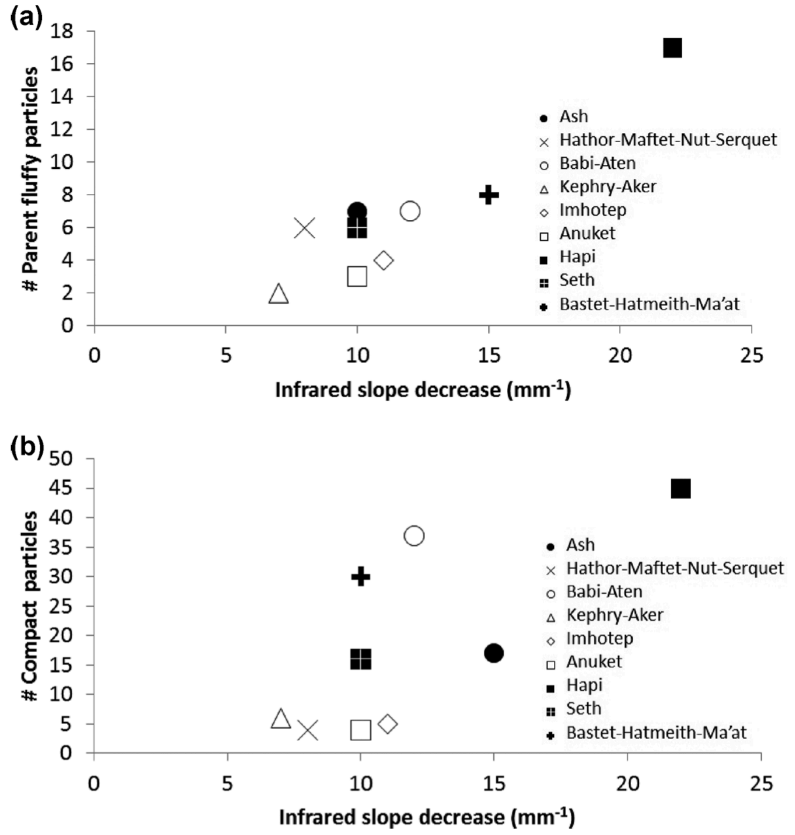

Figure 9. Number of fluffy parent (top) and compact (bottom) particles ejected from each nucleus region as a function of the *S* decrease measured by VIRTIS. Each symbol corresponds to a geomorphological region: in particular, circles, and triangles to body, diamond to bottom, mathematical symbols to head, and squares to neck regions.

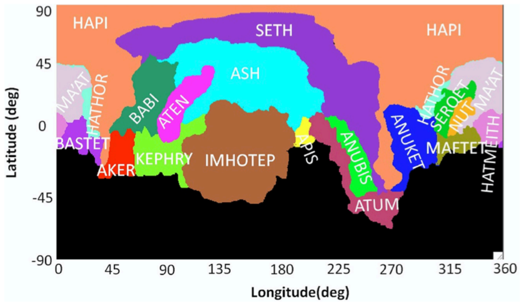

Figure 1. Cylindrical map of 67P/CG's 19 geomorphological regions as defined by El-Maarry et al. (2015) and Thomas et al. (2015).

On the VIRTIS side, we observed the change of the 3.2 μm band centre and of the spectral slope between 1.1 and 1.9 μm, between the lowest and the highest temperature measured from each region. The obtained decreasing trends are related to exposition of water ice, due to dust release.

On the GIADA side, we developed a trace back algorithm, based on measured dust particle speeds, outcomes of coma dust models (Ivanovski et al. 2017; Zakharov et al. 2018) and comet rotation, to obtain the number of fluffy and compact particles ejected from each region.

Conclusions:

(i) The ejection of fluffy parent and compact particles is correlated on the nucleus but not in the coma: the two particles types are emitted contemporarily from common nucleus surface areas, and they are later spread during the motion due to their different velocities.

(ii) All cometary activity indicators identify the neck (Hapi, Seth) and the body (Ash, Babi, Aten) regions as the most active.

Due to Sharing Geoscience Online format of EGU 2020 only selected recently published results (2019/2020) are displayed in this presentation

How comets work: nucleus erosion versus dehydration

Fulle et al. 2020, MNRAS

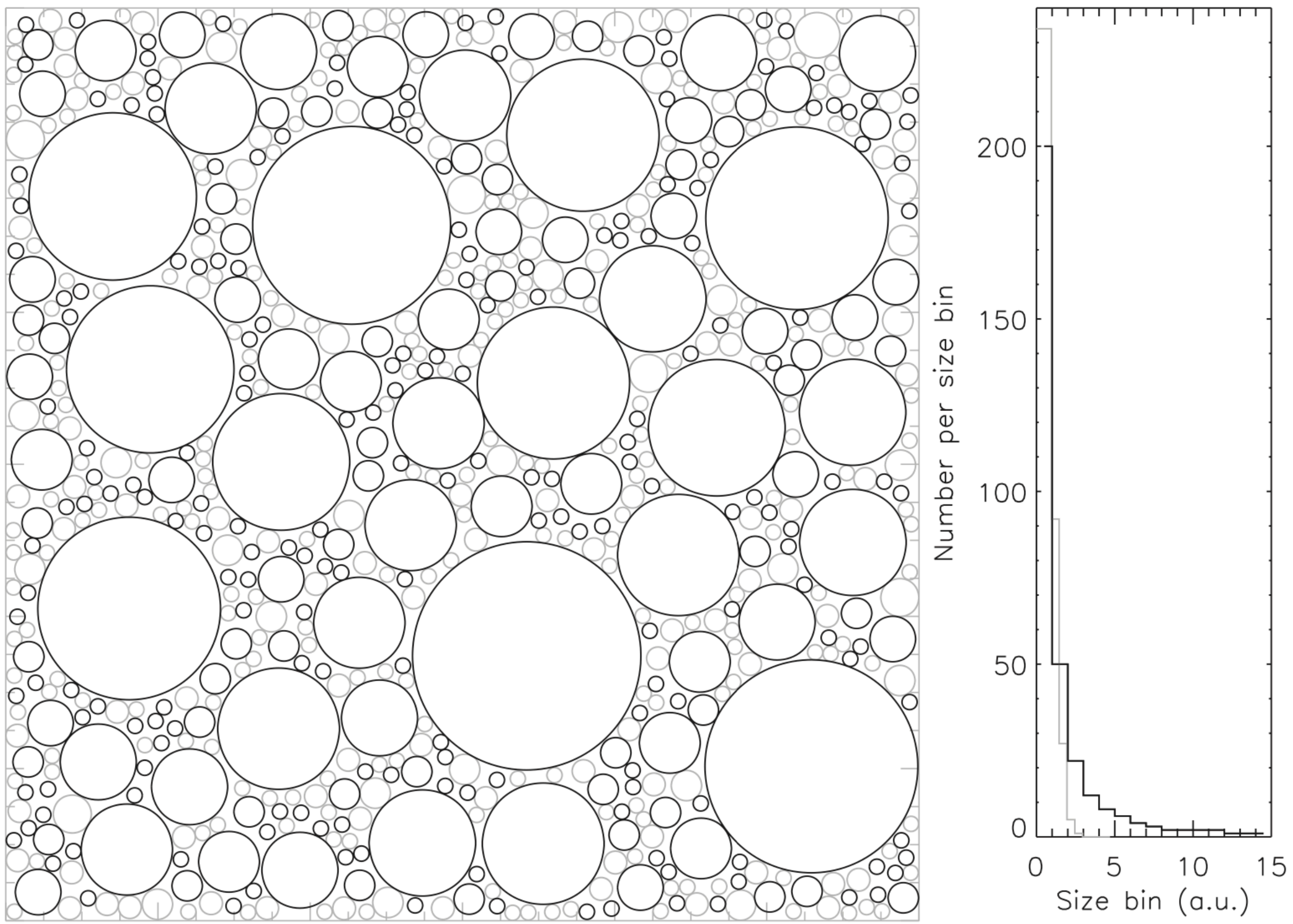

Figure 1. Subset of a non-homogeneous 2D loose-packed pebble composed of dust particles (black circles, left-hand panel) characterized by the differential size distribution with power index −2 (black histogram, right-hand panel). The largest possible circles filling the voids among dust particles define the pores (grey circles, left-hand panel) characterized by a steeper size distribution (grey histogram, right-hand panel) with power index ≈−4. Pores smaller than the smallest dust particles are not shown in this case. 3D models of close-packed spheres with a power index of −3 of the differential size distribution provide a steeper pore size distribution (power index ≈−6).

(i) The nucleus erosion rate and the water vapour flux are independent of the refractory-to-water-ice mass ratio, which affects the dehydration rate only.

(ii) The gas pressure inside the pebbles depends on the temperature only, and is >1 kPa at 67P perihelion.

(iii) The water vapour flux depends on the temperature and on the ratio between the monomer and pebble sizes, fitting the 67P water-loss rate data during the northern and southern polar summers if the active 67P surface is ≈5 km^2.

(iv) The smallest and largest ejected dust sizes depend on the nucleus surface temperature and its gradient at depths of a few cm inside the nucleus. Their computed values are consistent with the 67P dust ejection data.

(v) The water-driven nucleus erosion rate depends on the pebble heat conductivity, the average dust bulk density, the pebble heat capacity, and the largest ejected dust size. It is independent of the water vapour flux, implies no nucleus crust and fits the available 67P nucleus erosion data.

(vi) The nucleus dehydration is independent of the erosion rate and depends on the water vapour flux and the nucleus bulk density and refractory-to-water-ice mass ratio.

(vii) The different temperature dependences of the dehydration and erosion rates imply that 67P dm-sized chunks with a constant ice mass fraction behave in opposite ways at ejection and inbound to the following perihelion. At ejection, they are soon enveloped by an insulating crust, preserving most ice up to their fallout in Hapi. Inbound, the water-driven activity at low temperatures triggers a complete erosion of the fallout composed of chunks if their ice mass fraction is >0.1 per cent, explaining the 67P seasonal cycle.

(viii) >95 per cent of the southern pristine 67P nucleus, eroded to depths of ≈10 m (Fulle et al. 2019a; Gundlach et al. 2020), has a refractory-to-water-ice mass ratio >5, confirming independent results (Cambianica et al. 2020).

(ix) In 67P, the southern pristine nucleus is heterogeneous, with most water ice concentrated in <5 per cent of its volume, consistent with observations (Fornasier et al. 2019).

Composition | COSIMA | Stardust | ROSINA

Main question: is 67P solar or chondritic ?

- If carbonaceous chondrites(CC) are thought to have formed where the comet were formed, why the former contain all water in phyllosilicates, while the latter do not contain phyllosilicates?

- Origin of life: comets contain organic compounds and water locked up in their mineral structure. Comets contain aminoacids, some of the building blocks of proteins and DNA.

  - Stardust results baised due to the impact of high velocity and loss of material
  - COSIMA results biased by possible C contamination
  - A future cometary sample-return mission

Message: A sample return mission will be the best option.

3D+t dust modelling

Marschall, R. et al. 2019, Icarus
A comparison of multiple Rosetta data sets and 3D model calculations of 67P/Churyumov-Gerasimenko coma around equinox (May 2015)

Zakharov, V. V. et al. 2018, Icarus
Asymptotics for spherical particle motion in a spherically expanding flow

Skorov, Yu et al. 2018,MNRAS
Dynamical properties and acceleration of hierarchical dust in the vicinity of comet 67P/Churyumov-Gerasimenko

Ivanovski, S. L. et al. 2017, Icarus
Dynamics of non-spherical dust in the coma of 67P/Churyumov- Gerasimenko constrained by GIADA and ROSINA data.

Due to Sharing Geoscience Online format of EGU 2020 only selected recently published results (2019/2020) are displayed in this presentation

6 May 2020, S. Ivanovski, EGU2020

Diurnal Variation of Dust and Gas Production in 67P/ C-G

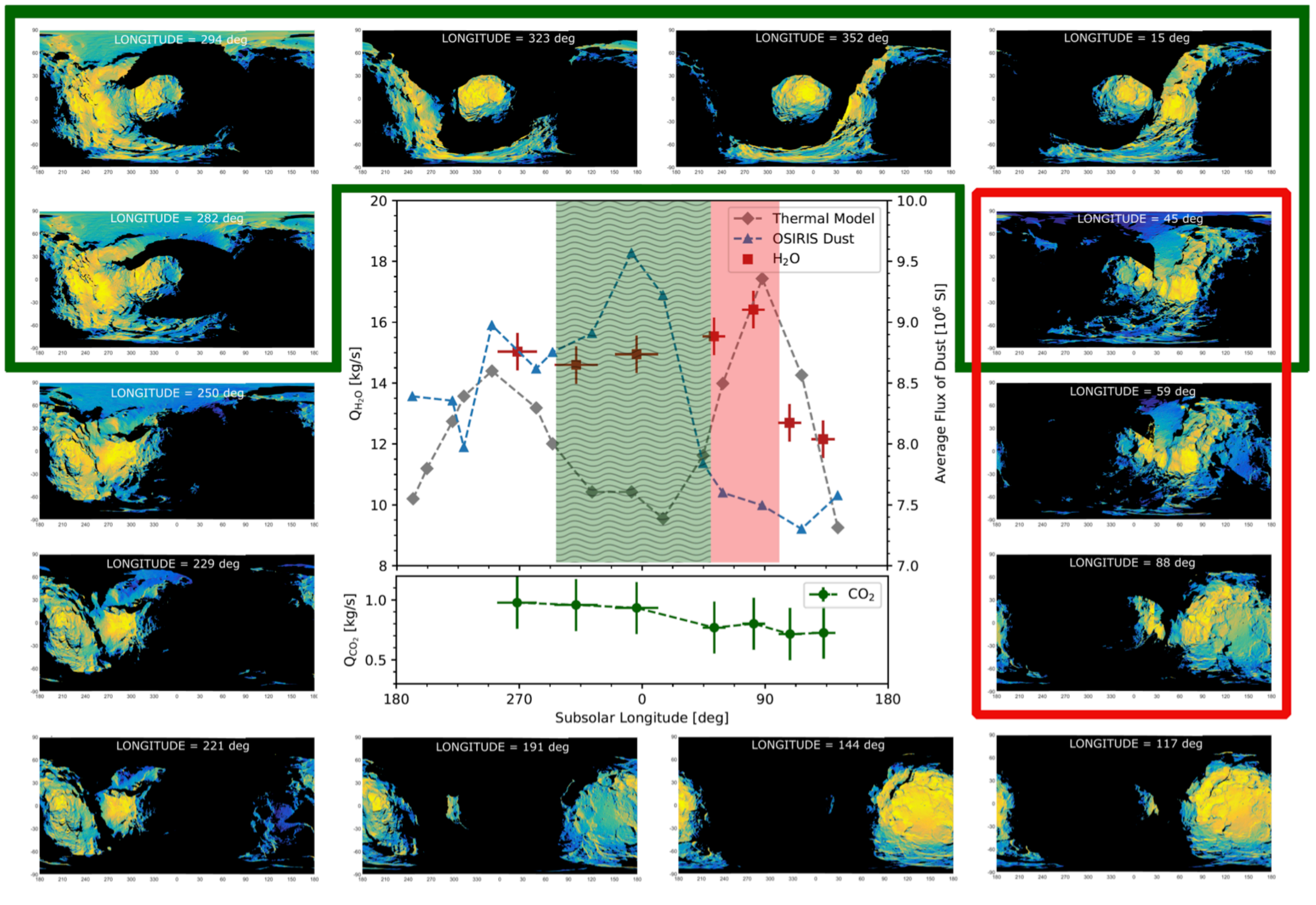

Fig. 10. Insolation maps for the time of each OSIRIS observation. Inset: total dust brightness and gas production rates, measured in the full 3.1 km annulus, as functions of subsolar longitude. The green box encloses the insolation maps that correspond to the subsolar longitudes where an excess of measured water production was found, relative to a simple model. The red box frames the insolation maps that correspond to the subsolar longitudes where a minimum of dust and a maximum of water production were measured.

Tubiana et al. 2019, A&A

Diurnal variation of dust and gas production in comet 67P/Churyumov-Gerasimenko at the inbound equinox as seen by OSIRIS and VIRTIS-M on board Rosetta

These observations show that when 67P is approaching perihelion, the dust activity cannot be understood based on water-driven activity alone.

Due to Sharing Geoscience Online format of EGU 2020 only selected recently published results (2019/2020) are displayed in this presentation

6 May 2020, S. Ivanovski, EGU2020

Ground-based observations

The ground-based dataset: overview and open questions (Courtesy: Colin Snodgrass)

Results so far

- Gas production – very asymmetric, appears to be linked with seasons
  - We see CN only when southern hemisphere illuminated
- Phase function agrees (over region measured) with Rosetta result
- Total dust production smoothly varying and repetitive from orbit to orbit
- No significant outbursts, or obvious link with ‘summer fireworks’
  - Maybe some change in large scale coma morphology? Related to late August 2015 events?

  Moreno et al. 2017, MNRAS

Snodgrass et al 2017, Phil.Trans.Royal Soc. A

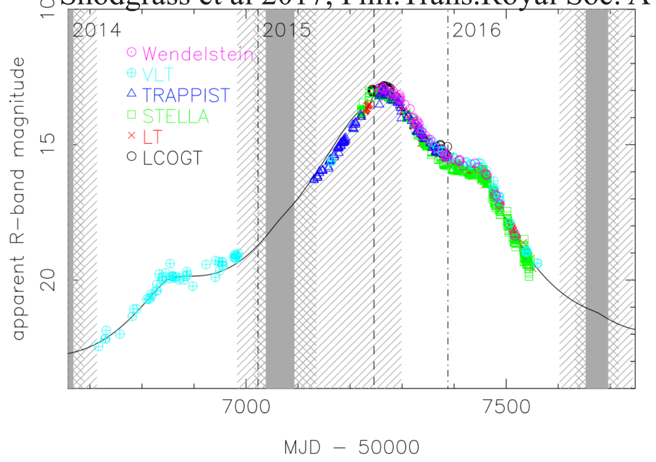

Opitom et al 2017, MNRAS

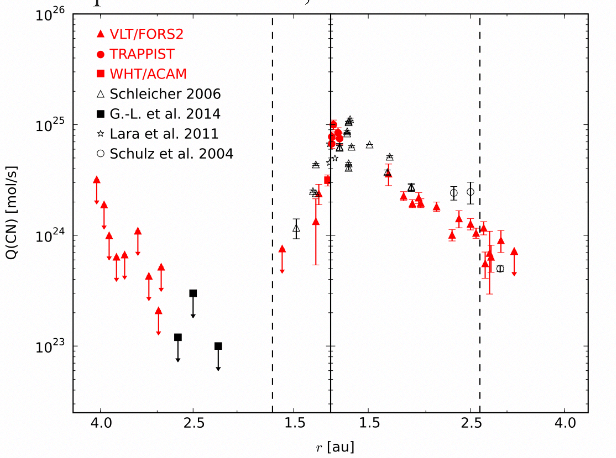

Questions

- How to link scales?
- Are large scale structures controlled by nucleus shape?
- Important to link Rosetta and ground

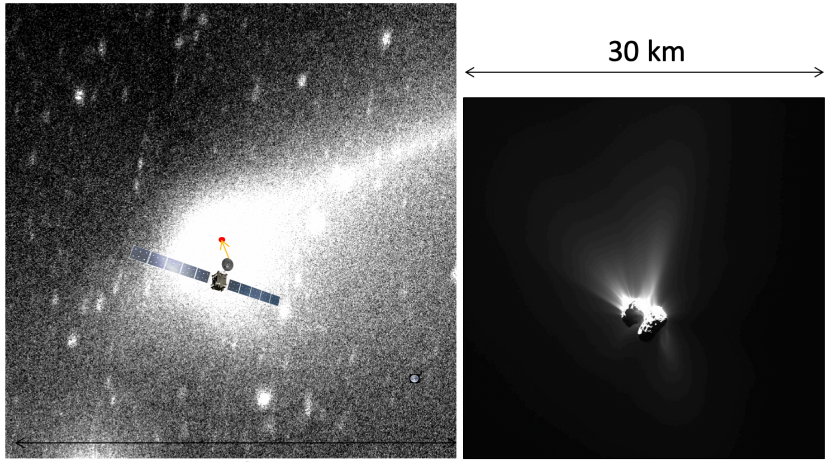

Boehnhardt et al 2016, MNRAS

- One approach: forward simulation from nucleus to coma scales

Summary

COSIMA ROSINA
Isotopic Ratios → D/H ratio …

Composition ROSINA
COSIMA VIRTIS ↔ Stardust

MIDAS
Grain Size Distribution

COSIMA
Structure and Porosity GIADA
MIDAS

IDP subunits

Albedo (opt. properties) GIADA
COSIMA OSIRIS VIRTIS

Thermal Properties
VIRTIS

Ground-based observations

Modelling

DNA of a Rosetta Dust Scientist

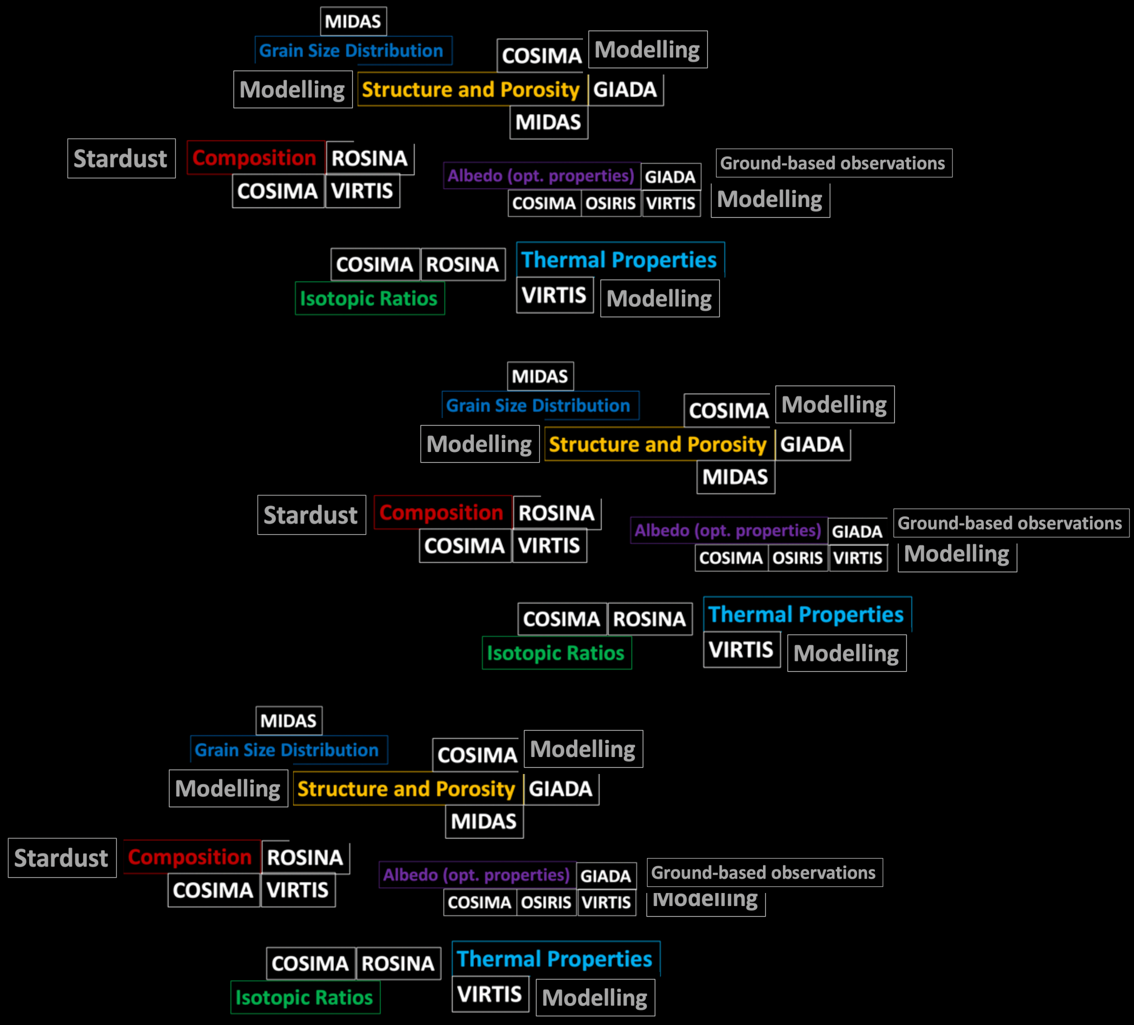

6 May 2020, S. Ivanovski, EGU2020